Particle production, transport, and identification in the regime of 1–7 GeV/c

A. C. Booth,[1] N. Charitonidis,[2,*] P. Chatzidaki,[2,3,4] Y. Karyotakis,[5] E. Nowak,[2,6] I. Ortega-Ruiz,[2] M. Rosenthal,[2] and P. Sala[2,7]

[1]*University of Sussex, Brighton BN1 9RH, United Kingdom*
[2]*CERN, 1211 Geneva 23, Switzerland*
[3]*National Technical University of Athens, School of Applied Physics, GR-157 80 Zografos, Attiki, Greece*
[4]*Heidelberg University, Kirchhoff-Institute for Physics, Im Neuenheimer Feld 227 D-69120 Heidelberg, Germany*
[5]*LAPP, Lab. d'Annecy-le-Vieux de Physique de Particules, Université Grenoble Alpes, Université Savoie Mont Blanc, CNRS/IN2P3, F-74941 Annecy, France*
[6]*AGH University of Science and Technology, Faculty of Physics and Applied Computer Science, al. Mickiewicza 30, 30-059 Krakow, Poland*
[7]*INFN, Via G. Celoria, 16 IT-20133 Milan, Italy*

(Received 13 March 2019; published 21 June 2019)

The recently constructed H4-VLE beam line, a tertiary extension branch of the existing H4 beam line in the CERN North Area, was commissioned in October 2018. The beam line was designed with the purpose of providing very low energy (VLE) hadrons and positrons to the NP-04 experiment, in the momentum range of 1–7 GeV/c. The production of these low-energy particles is achieved with a mixed hadron (pions, kaons, protons), 80 GeV/c secondary beam impinging on a thick target. The H4-VLE beam line has been instrumented with prototype scintillating fiber detectors providing the beam profile, intensity, and time-of-flight measurement of the beam particles, that, together with Cherenkov threshold counters, permit an event-by-event particle identification over the entire momentum spectrum. In this paper, we present detailed results of the beam line performance and the measured beam composition, as well as the comparison of these measurements with simulations performed during the design phase using FLUKA and GEANT-4-based Monte-Carlo codes.

DOI: 10.1103/PhysRevAccelBeams.22.061003

I. INTRODUCTION

The production of secondary hadron or lepton beams via the interaction of a primary beam impinging on a target material is the most common technique worldwide for providing experiments or facilities with particle beams of different intensities, compositions and momenta. A prominent example of a facility that provides mixed particle beams in the momentum range of 10 to 400 GeV/c is the CERN North Area Secondary Beam facility (see for example, Ref. [1]), where the primary beam from the CERN Super Proton Synchroton (SPS) accelerator impinges on a beryllium target and produces the secondary particles. During the 1980s, in a landmark article, H. Atherton *et al.* [2] measured the exact composition of secondary particles emitted from the CERN North Area beryllium targets, for different production angles, using the H2 beam line. The lowest secondary momentum point reported by Atherton *et al.* is 60 GeV/c, in both positive and negative polarities. The work, described in Ref. [2], was subsequently supplemented by the NA-56/SPY experiment [3], that performed measurements of secondary particle production down to 7 GeV/c, starting this time from 450 GeV/c primary protons and impinging on beryllium targets of different lengths. However, data for secondary particle production below 7 GeV/c starting from medium-to-high momenta (in the multi-GeV/c range) and for target materials different than beryllium are, to the authors' best knowledge, quite scarce and difficult to find in the literature.

The recently commissioned NP-04 (Single-Phase ProtoDUNE) experiment [4], located in an extension of the CERN North Area EHN1 facility designated "CERN Neutrino Platform Facility" [5], is a large-sized prototype detector based on Liquid Argon Time Projection Chamber (LAr–TPC) technology. As described in the experiment's

*Corresponding author.
nikolaos.charitonidis@cern.ch

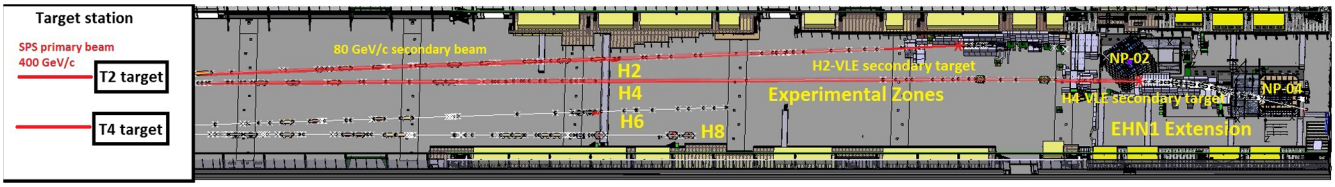

FIG. 1. A schematic layout of EHN1, the largest experimental hall of SPS secondary beam facilities. As explained in the text, the primary beam from SPS is slowly extracted on the primary (T2) target. Subsequently, the secondary 80 GeV/c beam is momentum-selected and transported to the newly constructed secondary targets, in order to produce the low energy particles. The newly designed H2-VLE and H4-VLE beam lines select and transport these low energy particles to NP-02 and NP-04 experiments.

scientific proposal, and also justified in detail in the DUNE technical design report [6], the hadrons produced by neutrino interactions with matter are expected to be in the range between 0.5 and 10 GeV/c. In order to satisfy these requirements, a new tertiary branch of the existing H4 beam line was designed during 2017 with the installation and commissioning to take place in 2018. The layout and optics design principles of these new beam lines have been reported elsewhere [7]. The conceptual design of the beam line involves a medium-energy, medium-intensity (10^6 particles per 4.8 seconds spill) secondary beam of 80 GeV/c produced in the T2 "primary" target and transported to impinge on a "secondary" target. The new H4-VLE beam line accepts, momentum-selects and transports the third generation ("tertiary") low-energy particles to the NP-04 experiment. A layout of the EHN1 facility showing the existing and the new beam lines can be seen in Fig. 1.

In this paper, we present in detail the methodology for the optimization of this low energy beam line in terms of beam optics, target material choices as well as radiation shielding. The transverse dynamics studies were performed with various beam optics and tracking codes, while the particles' interactions with matter were studied using well established Monte-Carlo codes. Furthermore, we discuss the instrumentation and particle identification systems chosen. We finally report on measurements of the particle production rates and relative abundance in the momentum regime of interest of 1–7 GeV/c, along with a comparison to Monte-Carlo simulations.

II. OPTIMIZATION SIMULATIONS

A. Optics and target optimization

As discussed in Ref. [7], low energy particles are produced via a secondary beam with a momentum of 80 GeV/c, which is generated in the existing T2 target and transported for ~600 m through the H4 beam line towards a secondary target. The design of the tertiary beam line after this target had to satisfy the following stringent requirements: (a) relatively short length (to limit the amount of pion and kaon decays upstream of the experiment) (b) large bending angles (to avoid the high-energy background reaching the experiment), and (c) large angular acceptance (at least in the order of 50 mm mrad), in order to assure sufficient rate for the experiment. The initial optics configuration ("v0") discussed in the reference above, was chosen as a first estimate, using the first-order optics calculation code TRANSPORT [8]. Despite the broad use of this code in the experimental areas of CERN and elsewhere since the 1970s, it presents a few intrinsic limitations: (a) It is not possible to restrict the minimum and maximum value of any fit parameter (b) The fitting algorithm is not optimal, thus leading to an important dependence of the possible solution on the initial value used for the fit. This fact allows only families of optics solutions to be found without offering the ability to easily explore large parameter phase-space domains. (c) Since the spatial and momentum coordinates of the produced particles are highly correlated, tracking through the magnetic elements with a realistic phase space as input was deemed necessary. This option is not offered by TRANSPORT or its associated tracking tool, DECAY TURTLE [9]. Additionally, there is no possibility of communication of variables between the optics and the tracking programs. (d) The results processing, in terms of the output file format in conjunction with the various intrinsic limitations of FORTRAN (for example, in character manipulation), can become inconvenient especially in the cases that a large parameter variation is necessary.

In order to overcome these challenges and at the same time explore the possibilities that modern optics and Monte-Carlo programs offer for matter-dominated beam lines, the following strategy was employed:

(a) The preexisting H4 beam line and the H4-VLE part were modeled in the GEANT-4 based Monte-Carlo program G4beamline [10]. The model included a detailed description of the magnetic elements' geometrical features and materials, while for the crucial H4-VLE part, their magnetic fields (inside the magnets' gap, the iron yokes as well as the fringe fields), were modeled via explicitly calculated field maps. All the collimators and most of the detectors of the upstream, high-energy beam line were also modeled, along with all the relevant part of the shielding. All the detectors, vacuum windows, and material present in the particles' trajectories were modeled precisely in the H4-VLE low-energy part.

(b) The expected secondary beam composition at 80 GeV/c, as predicted by the "Atherton formula"

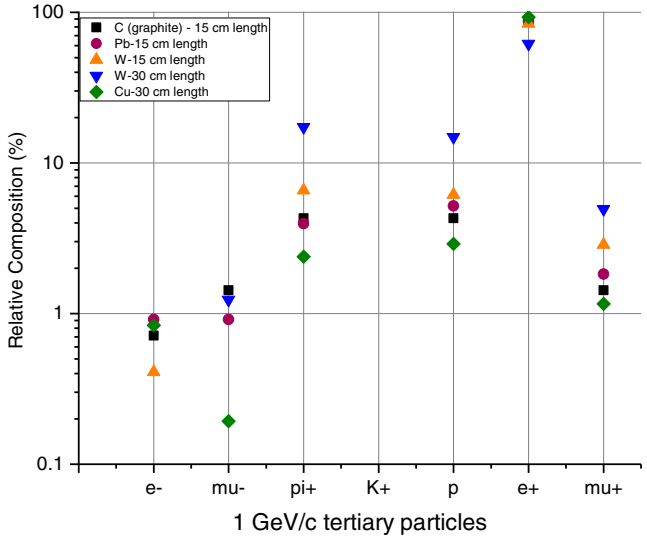

FIG. 2. Target optimization simulations, performed with G4beamline. It is shown that 30 cm of tungsten provides better absorption of the positrons, thus leading to an increased relative amount of pions and protons for the low energy beams of 1, 2 and 3 GeV/c, as discussed in the text.

(described in Ref. [2]) was generated at the position of the T2 target and transported over ∼600 m to the secondary target. The secondary target material was optimized using G4beamline simulations (with the FTFP_BERT physics list), and the results are shown in Fig. 2. A tungsten target, 30 cm in length and 50 cm in radius was chosen for the lower part of the momentum spectrum (up to 3 GeV/c), while a copper target with the same dimensions was chosen for the higher part of the momentum range (above 3 GeV/c). This choice was made to increase the beam hadron content in the lower part of the momentum range, where the production is dominated by electrons. The low energy particles produced were scored just after the target, and their species along with their angular and momentum coordinates were recorded in a ROOT [11] file.

(c) This "emittance" of particles was used as input to a custom-made, combined *Mathematica*® [12] (a powerful technical computing framework), MAD-X [13] (a modern optics code, developed at CERN and broadly used internationally), and PTC [14] (an independent library compatible with MAD-X, offering tracking based on symplectic integration) interface. The developed technique is described in detail in Ref. [15]. MAD-X offers a great degree of flexibility in the fitting algorithms and the possible output formats. In addition, PTC takes into account higher-order effects (including kinematic coupling, high-order dispersion or chromatic aberration effects, etc.) as well as the magnet fringe field effects up to second order, as described in [16,17]. Moreover, it allows a convenient exchange of parameters between the different optics solutions and the tracking module. An iterative optimization process was

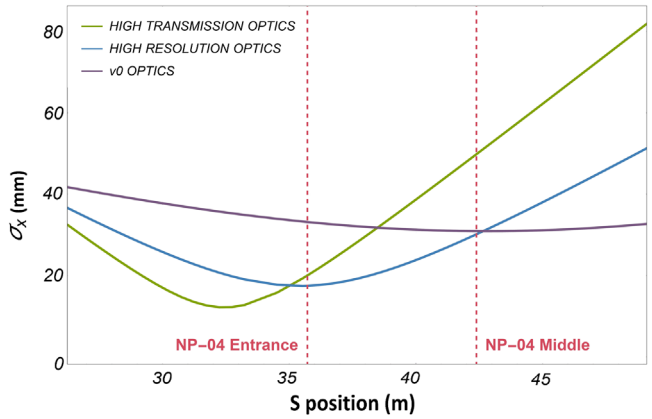

FIG. 3. Bending plane beam size in H4-VLE near the detector entrance for a 7 GeV/c beam, as simulated via PTC. It is shown that in the bending plane, the high-transmission optics results in a much smaller spot-size at the NP-04 entrance, at the expense of a bigger spot-size at the middle of the cryostat. The high resolution optics gives even smaller spot size at the entrance and the center of the cryostat, at the expense of the rate, as discussed in the text.

performed using the "realistic" estimation of the particles' phase-space generated at the target by G4beamline.

This procedure led to two new optical modes: A "high-transmission" mode, maximizing the particle rate at the experiment, and a "high-resolution" mode, which minimizes the spot size at the same position. The results of the study, demonstrating the differences of the new optical modes in the beam waist with respect to the first version (v0) are summarized in Fig. 3 for the bending plane and in Fig. 4 for the nonbending plane.

Both high-transmission and high-resolution optics provide a significant spot size reduction at the entrance of the cryostat in the bending plane compared to v0 optics.

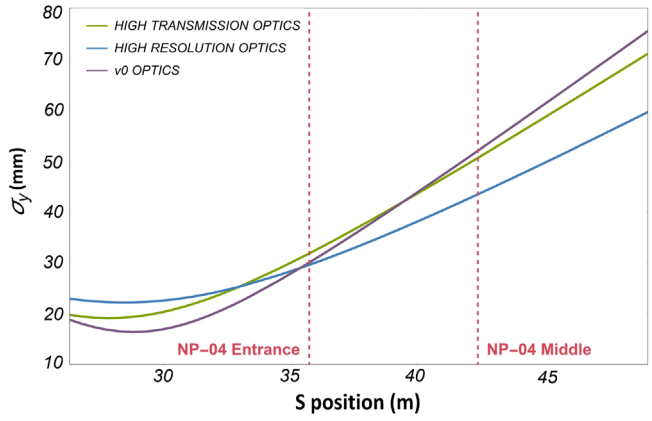

FIG. 4. Nonbending plane beam size in H4-VLE near the detector entrance for a 7 GeV/c beam, as simulated via PTC. In the nonbending plane, the high-transmission optics gives a better rate with small difference in the spot size, whereas the high resolution optics gives even smaller spot size at the entrance and the center of the cryostat, compared to v0 optics.

Specifically there is a ∼16 mm spot size reduction when using the high-resolution optics (corresponding to 40 %, compared to v0 optics) and a ∼13 mm reduction in high-transmission optics compared to the initial calculations, preserving the large angular acceptance of the beamline, equal to 10 mrad in both the bending and the nonbending planes. The high-transmission optics achieves through a better control of the nonbending plane, a ∼15 % higher transmission compared to v0 optics. Both new optical modes offer a sufficient rate for the experiment as well as the necessary flexibility for different focusing configurations. The tracking results for the new optical modes as calculated by PTC were compared with G4beamline (using field maps for the bending magnets, calculated with OPERA3D [18]) and a very satisfactory agreement was found both in terms of overall transmission and transverse profiles, as discussed in Ref. [15].

B. Misalignments study

The bending magnets of the H4-VLE beam line are tilted by 56.75° clockwise, and the quadrupoles by 33.25° counterclockwise (for reasons discussed in Ref. [7]). At the same time, the short length of the beam line prohibits the installation of any corrector magnet. It was therefore deemed necessary to study in a detailed manner all the possible misaligments of the magnetic elements and understand their effect on the beam. The misalignment types taken into account in this study were longitudinal, angular, or transverse. In the latter case assuming a misplacement of the magnet on its support, or the misplacement of the entire support.

In order to reduce the statistical error and follow a pragmatic approach, for every misalignment type studied, 500 different runs were performed, each introducing a random misalignment, conservatively chosen, normally distributed around the nominal position. The standard deviations chosen were $\sigma = 0.5°$ for the angular misalignment types and $\sigma = 0.5$ mm for the spatial misalignment types. Each magnetic element was then "randomly" placed, and tracking was then performed with PTC. This sensitivity

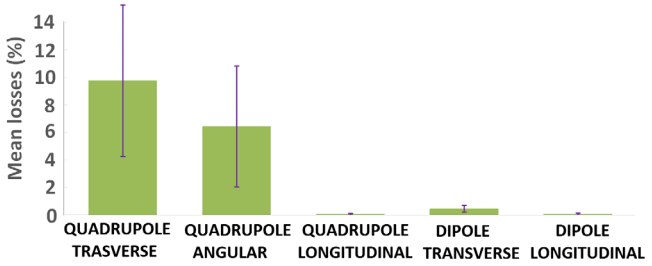

FIG. 5. Simulated mean losses of various misalignment types for H4-VLE. The misalignments studied had a Gaussian distribution with a σ of 0.5 mm for spatial and 0.5° for angular misalignments. The transverse and angular misalignments of the quadrupoles affect the particle transmission the most.

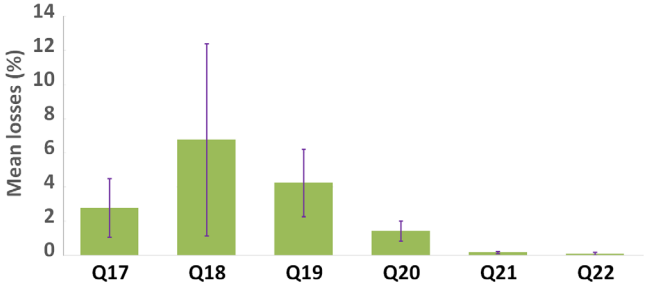

FIG. 6. Transverse misalignment effect on beam losses for each quadrupole of H4-VLE. It is seen that a possible Q18 misalignment has an important effect on the beam losses.

analysis, presented in Fig. 5, affirms that the particle losses are higher in case of transverse or angular quadrupole misalignments, compared to all the other types of misalignments.

Following the result of the first analysis, the study subsequently focused on discriminating which quadrupoles the beam characteristics are most sensitive to. The effects of the misaligments for each quadrupole of H4-VLE, keeping the rest in their nominal position, are shown in Fig. 6. It can be seen that the particle rate is mostly sensitive

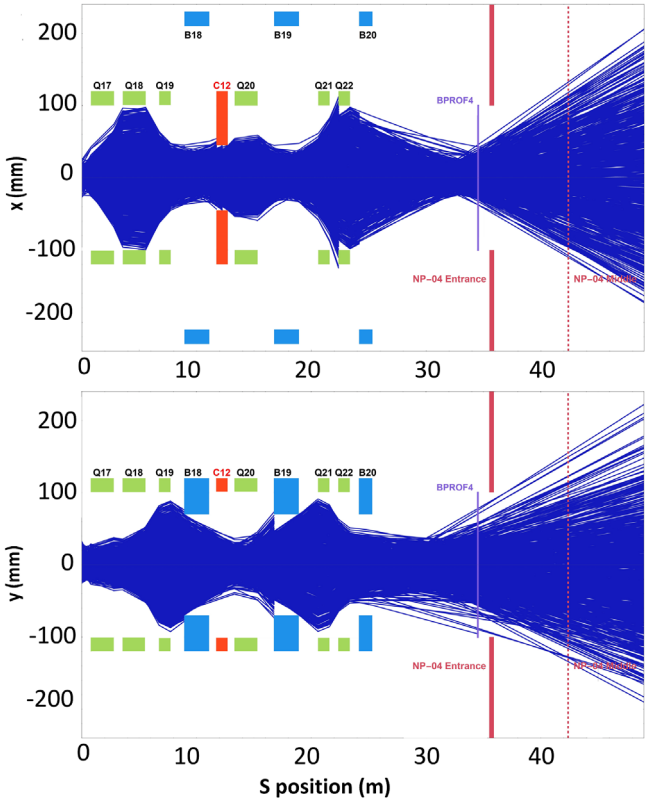

FIG. 7. Transverse profile of the beam in the bending (top) and nonbending (bottom) plane, assuming a misalignment of Q18 by 1 mm, as simulated for a 7 GeV/c beam in PTC, using the high-transmission optics. Losses occur mainly in the collimator and the quadrupole apertures for the bending plane, while, for the nonbending plane, in the bending magnets' apertures.

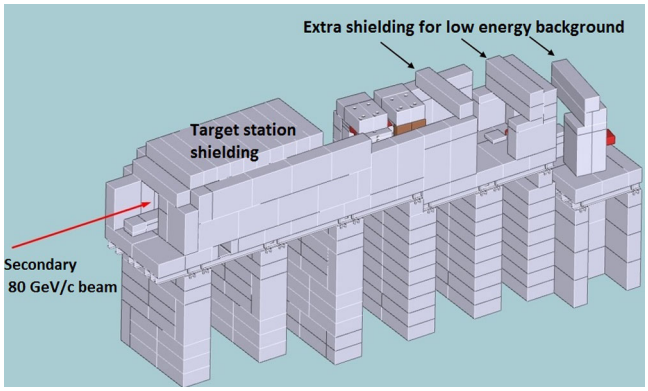

FIG. 8. Final design of the shielding of the H4-VLE beam line, after optimization with FLUKA.

to the second quadrupole of the acceptance triplet, as expected from the high value of the β-function at this quadrupole and the strength of the magnet.

The profile of the beam, assuming a transverse misalignment of the second quadrupole magnet by 1 mm, is illustrated in Fig. 7. Based on the above analysis, particular attention was given to Q18 and Q19 during the installation process, reassuring a placement precision of below 1 mm in both the longitudinal and the transverse planes, in order to keep the expected losses under control and avoid them becoming a show-stopper for the experiment.

C. Shielding optimization

As already mentioned in the previous sections, NP-04 is a Liquid Argon TPC detector and as such, is limited by slow read-out (normally in the regime of a few tens of Hz). For this reason, the beam-induced background had to be minimized. Detailed simulations using the FLUKA [19,20] Monte-Carlo code were performed in order to eliminate the main background sources, namely the medium-energy muons originating from secondary pion and kaon decays in the last straight-section of the existing H4 beam line, or low energy hadrons and muons created by interactions in the beam line elements and apertures. The final design of the shielding is shown in Fig. 8. The simulated fluence of all charged particles impinging on the front face of the NP-04 detector, in the case that the low-energy beam line is tuned to transport 7 GeV/c particles, is shown in Fig. 9. This shielding optimization resulted in a drastic reduction of the background to the order ~600 Hz for charged particles and to ~1.2 kHz for neutrons, per 10^6 particles impinging on the secondary target, for the case of 7 GeV/c.

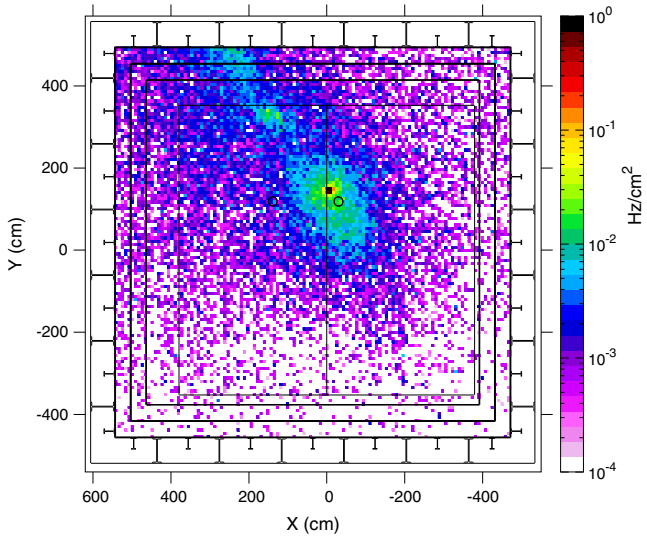

FIG. 9. All charged particles fluence impinging on the front face of the NP-04 detector. The the beam spot is shown around (0, 150), while the small hole next to it represents the entrance of the beam in the TPC active volume. A halo produced by a tail of high-energy particles, deflected in the higher-part of the cryostat can be also seen.

III. BEAM INSTRUMENTATION AND PID

An overview of the beam line instrumentation is shown in Fig. 10. The beam line is equipped with profile monitors ("XBPF"), shown as green vertical lines, trigger counters ("XBTF"), shown as red vertical lines and two threshold Cherenkov counters ("XCET"), one able to sustain a high-pressure radiator gas, up to 15 bar and a second one able to sustain gases with lower pressures (up to 5 bar). The blue triangles represent the beam line bending magnets, that define the reference beam trajectory. A more detailed description on the selected instrumentation and its performance follows in the next paragraphs.

A. Profile monitors and trigger planes

The profile monitors ("XBPF"), described in Ref. [21], consist of 192 square scintillating fibers, each with a thickness of ~1 mm, packed in a planar configuration and covering a surface of about 20×20 cm^2. On the bottom part of the structure, a high-reflectivity aluminized mylar mirror is glued. On the other end, an individual Hammamatsu S13360-1350 silicon photomultiplier (SiPM) is reading the signal from each fiber. The fiber structure is located inside a vacuum tank, thus avoiding the particle

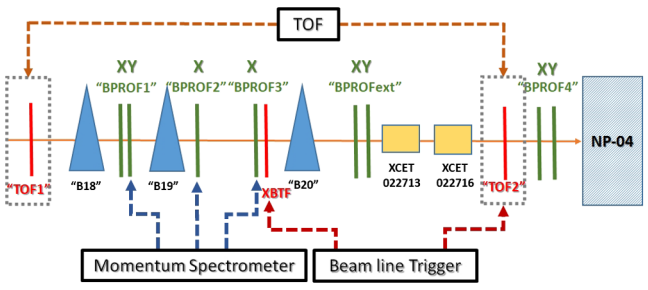

FIG. 10. An overview of the H4-VLE instrumentation, as discussed in the text.

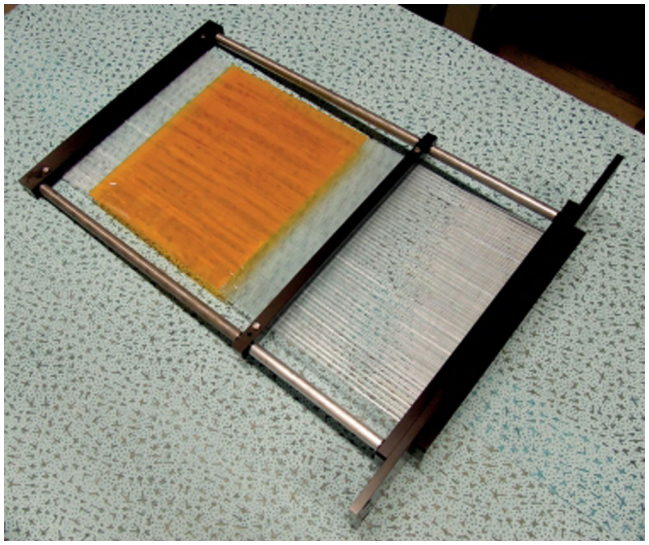

FIG. 11. XBPF module, used as beam profile monitors. The fibers are read out by 192 SiPMs coupled with CITIROC ASICs, that transfer the signal to the back-end VFC as discussed in the text.

interactions with the air molecules. The signal is collected through a front-end board, comprising 6 CITIROC application-specific integrated circuits (ASIC), that process and discriminate the SiPM signals. The discriminated digital output is sent via a Xilinx field programmable gate array (FPGA) to the back-end VME-FMC carrier (VFC) board, a Versa Modula Europa (VME) digital acquisition electronics system that communicates control data and decodes the data stream arriving from the front-end board. The VFC is fully compatible with the White Rabbit technology [22] that has been chosen for the timing information of the events with sub-ns accuracy, also for the NP-04 detector.

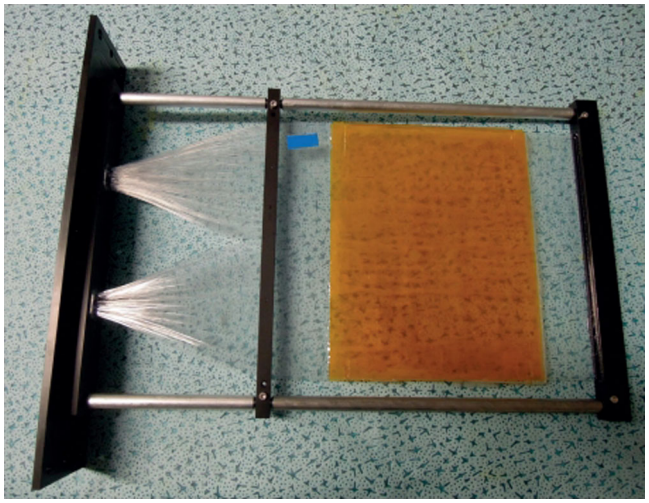

FIG. 12. XBTF module. The fibers are grouped in two clusters which are read-out through conventional PMTs. The coincidence signal of the three XBTFs is forming the beam trigger, which is sent to the experiment as well as to the XBPF monitors.

The trigger planes ("XBTF") are of very similar conceptual design, with the main difference being that the fibers are grouped in two bundles, while the readout is done via two "conventional" photomultipliers (PMTs) (Hammamatsu H11934-200). The analog signals from the two downstream XBTFs are sent to a programmable delay module that puts them in a two-fold coincidence. The trigger signal is then sent to the experiment as well as to the backend electronics of the XBPF modules. The two different modules are shown in Figs. 11 and 12. Using the XBPFs and the XBTFs, every trigger event is being precisely timestamped using the White Rabbit common clock, shared between the beam instrumentation and the detector data acquisition (DAQ) system. In addition, the integrated beam intensity for all the trigger particles is measured and provided.

B. Time-Of-Flight (TOF)

A time-of-flight measurement system was implemented by connecting the signals from the upstream and downstream XBTFs, as shown in Fig. 10, to a time-to-digital converter (FMC-TDC [23]). The TDC was configured to use the reference White Rabbit clock in order to define timestamps on all the beam events, with a precision of 81 ps. The total resolution of the system has been measured offline to be ∼900 ps. The distance between the two trigger planes used for the time of flight is 28.575 m. An example of the particle identification performance at 1 GeV/c is shown in Figure 13.

C. Cherenkov detectors

The beam line was equipped with two kinds of threshold Cherenkov detectors, frequently used in many of the CERN

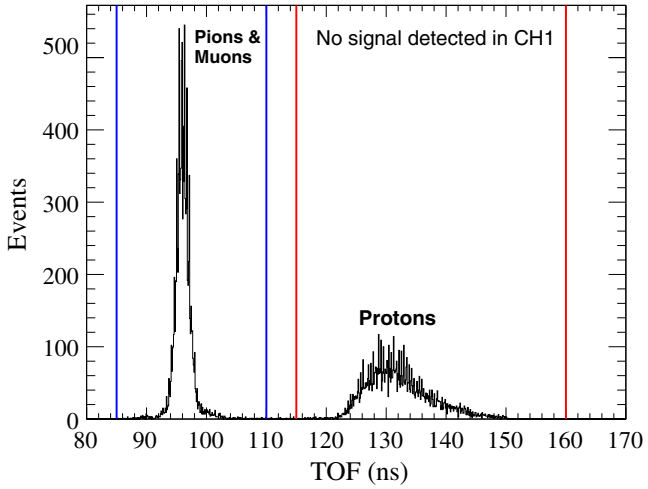

FIG. 13. Particle identification with the combined use of Cherenkovs and time of flight techniques. At 1 GeV/c, and when the low pressure Cherenkov does not give signal, pions/muons can be identified with a peak around 95 ns and protons around 130 ns.

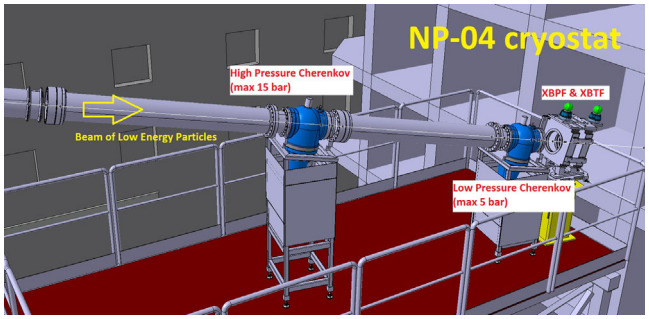

FIG. 14. The two Cherenkov detectors mounted in the H4-VLE beam line. One is able to sustain a radiator gas up to 15 bar and the other up to 5 bar. Inside the blue tank, a curved mirror deflects the Cherenkov photons created in the gas towards the photomultiplier located in the bottom of the detector.

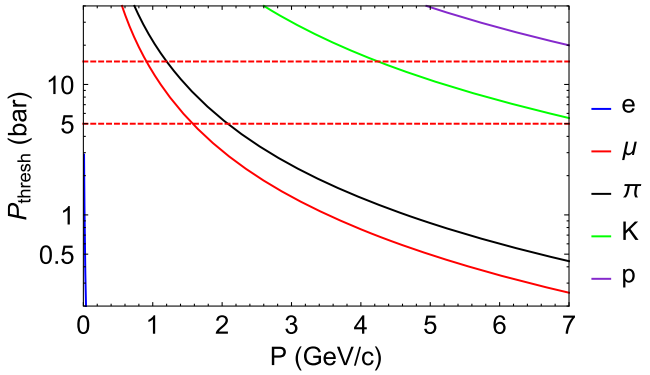

FIG. 15. Threshold pressures of CO_2, for the two Cherenkov detectors used in H4-VLE, for all the different particle species. The two maximum pressures of the Cherenkovs, 5 and 15 bars, are drawn as horizontal red dashed lines in the plot. As summarized in Table I and discussed in the text, positrons are always tagged via the first (low-pressure) Cherenkov, while in the higher momenta, using the high-pressure Cherenkov protons and kaons can be also identified.

experimental areas [24]. Both devices consist of a stainless steel "head," containing a curved mirror guiding the photons created in the gas towards a photomultiplier, which is located at the bottom of the device. A large tube (of 1.9 m length) allows for sufficient path length in the radiator gas, thus increasing the probability of the Cherenkov produced photons reaching the photomultiplier. A drawing of the two detectors mounted in the beam line, just before the NP-04 cryostat, is shown in Fig. 14.

The chosen radiator gas was CO_2, for reasons of simplicity and cost. In addition, given the unknown beam composition, this gas has been preferred due to its well-documented refractive index [25], allowing for faster tuning of the detectors. Moreover, at the momentum spectrum of interest, and as shown in Fig. 15, with a pressure up to 15 bar, the low energy positrons and pions can be tagged. For momenta above 5 GeV/c, and with higher pressures kaons and protons can be tagged as well. For momenta below 3 GeV/c, the time-of-flight technique is used instead. In order to provide timing information and allow for data analysis on an event-by-event basis, the analog Cherenkov signal was also sent to the TDC in Sec. III-B. A summary of the particle identification techniques is shown in Table I. Using the low-pressure Cherenkov ("CH1") at 1 & 2 GeV/c the positrons are tagged while muons and pions are flagged by setting the high-pressure detector ("CH2") below the proton threshold and the low pressure one above the positron threshold; at the higher momenta (6–7 GeV/c), kaons and protons can be distinguished by adjusting the pressure below the proton threshold. An example of the combined use of the Cherenkovs for 3 GeV/c momentum is shown in Fig. 16. The data points have been fitted with the formula $1 - e^{-N_{pe}}$, convoluted with a Gaussian momentum spread of 6 % for positrons and pions and 10 % for muons. N_{pe} is the average number of photoelectrons, given by Eq. (1):

$$N_{pe} = 2A \cdot L_{rad} \cdot (n-1) \cdot (P - P_{th}) \tag{1}$$

where it can be easily shown that the refractive index is related with the threshold pressure:

$$P_{th} = \frac{m^2}{2 \cdot (n-1) \cdot p^2} \tag{2}$$

In Eq. (1), L_{rad} is the length of the radiation volume, n the refractive index of the gas at 20 °C and 1 bar pressure. The parameter A constitutes an empirical constant,

TABLE I. A summary of the particle identification techniques used in H4-VLE, in order to assess the beam composition in all momenta.

p (GeV/c)	e	μ	π	K	p
1	CH1	TOF	TOF	/	TOF
2	CH1	TOF	TOF	/	TOF
3	CH1	CH2 & !CH1	CH2 & !CH1	TOF	TOF
4	CH1	CH2 & !CH1	CH2 & !CH1	TOF	TOF
5	CH1	CH1	CH1	CH2 & !CH1	!CH1 & !CH2
6	CH1	CH1	CH1	CH2 & !CH1	!CH1 & !CH2
7	CH1	CH1	CH1	CH2 & !CH1	!CH1 & !CH2

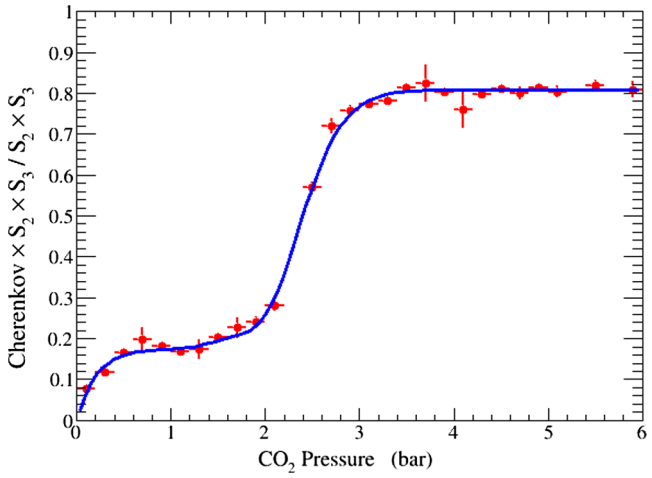

FIG. 16. Pressure scan demonstrating the particle identification using two Cherenkov counters, for the case of 3 GeV/c. The first plateau around 4 bar corresponds to pions and muons. The second plateau around 1 bar corresponds to positrons. Setting therefore one Cherenkov to 4 bar and the second to 1.2 bar, pions/muons and positrons are tagged.

depending on the wavelength of the emitted Cherenkov light, the efficiency of the optical system, the photon collection efficiency, the quantum efficiency of the photocathode and the discrimination threshold.

D. Momentum Spectrometer

As shown in Ref. [26], the momentum spread of the new beam line which is defined by its geometrical layout and transverse optics, has a standard deviation of 7 %, when the collimator is fully open. For a more precise determination of each particle's momentum, a momentum spectrometer consisting of three profile monitors around a dipole magnet was designed and implemented, using the XBPF detectors described in Sec. III. A. The operation of such a spectrometer has been tested in the past using wire chambers (see for example Ref. [27]), demonstrating a satisfactory performance. A schematic illustrating the principle is shown in Fig. 17, where the particle deflection angle and therefore its momentum can be determined using Eqs. (3) and (4).

$$\cos\theta = \frac{M\cdot[\Delta L\cdot\tan\theta_0 + \Delta\chi\cdot\cos\theta_0] + L_1\cdot\Delta L}{\sqrt{[M^2+L_1^2][(\Delta L\cdot\tan\theta_0+\Delta\chi\cdot\cos\theta_0)^2+\Delta L^2]}} \tag{3}$$

$$p = \frac{299.7924}{\theta}\times\int_0^{L_{\mathrm{mag}}}(B\cdot dl) \tag{4}$$

In the above equations, $\alpha = \frac{\chi_3\cdot L_2-\chi_2\cdot L_3}{L_3-L_2}\cdot\cos\theta_0$, $\Delta L \equiv L_3 - L_2$, $\Delta\chi \equiv \chi_2 - \chi_3$, $M \equiv \alpha + \chi_1$, and θ is the deflection angle of the spectrometer magnet, which is for the case of H4-VLE equal to 120.003 mrad for the reference particle.

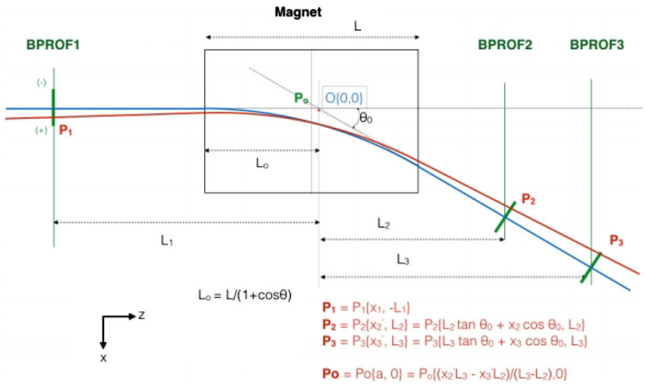

FIG. 17. Schematic of the spectrometer principle, taken from [26].

The energy loss due to synchrotron radiation effects, primarily affecting the positrons, equal to approximately 0.22 MeV/c for 7 GeV/c positrons, is considered negligible and has been neglected in this analysis. The resolution of this spectrometer is limited by the spatial resolution of the XBPFs. Given the fiber width of 1 mm, the resolution of the spectrometer has been calculated with Monte Carlo simulations to be equal to approximately 2.5 % [28].

IV. RESULTS

A. Momentum spread

The comparison between the measured and simulated momentum spread of the beam is shown in Fig. 18. The theoretical momentum bite ($\Delta p/p$) of the beam line, is defined by the layout and the first-order optics and has been calculated to have a σ of about ~7 %, being in a very good agreement with both the simulations and the measurements.

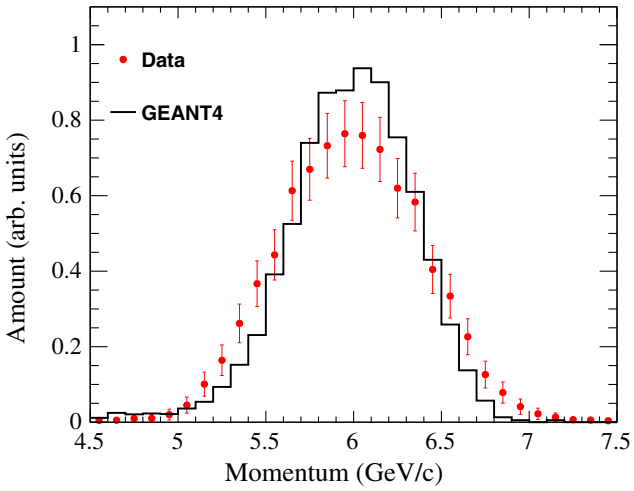

FIG. 18. Measured and simulated momentum spread for 6 GeV/c. A very good agreement with G4beamline is demonstrated. The Poissonian error bars have been multiplied by 10 for visualization reasons.

B. Beam composition and trigger rates

Combining all the aforementioned instrumentation, an analysis of all the beam particles was possible on an event-by-event basis, determining for each triggered particle its position at all profile monitors (XBPFs), its momentum via the spectrometer and its species using the Cherenkov detectors and the time-of-flight monitors. Data were collected in the range between 1 and 7 GeV/c, in steps of 1 GeV/c. The results have been normalized to 10^6 particles on the secondary target. The measured total trigger rates, compared with the simulated ones using FLUKA and G4beamline, are shown in Fig. 19. An agreement between measurements and simulations is demonstrated, both for the tungsten target (momenta ≤ 3 GeV/c) and the copper one (momenta > 3 GeV/c). A 95 % efficiency has been assumed for each trigger plane, resulting in a 90 % overall efficiency of the trigger. In Figure 20 the measured efficiency, calculated as the number of trigger events with at least one responding fiber hit divided by the number of general triggers, is shown for all the XBPF profile monitors.

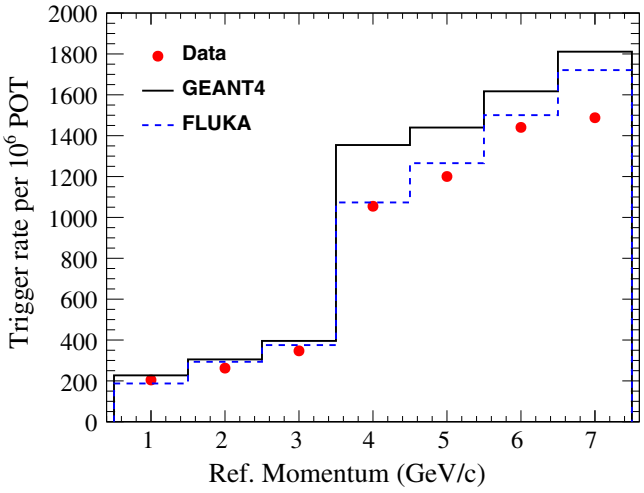

FIG. 19. Measured and simulated trigger rates, in all momenta. The W target has been used for the momenta ≤ 3 GeV/c and the Cu target for the momenta above 3 GeV/c. A 90 % overall trigger efficiency has been assumed, as discussed in the text.

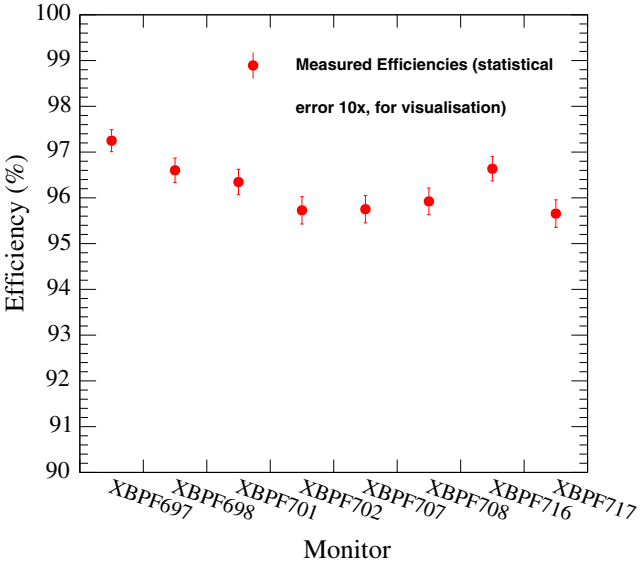

FIG. 20. Measured efficiencies of the fiber profile monitors, calculated as the number of trigger events with at least one channel hit, divided by the number of general triggers.

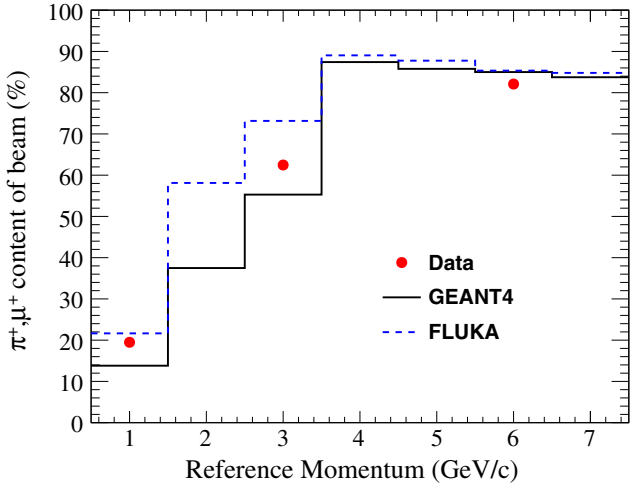

FIG. 21. Measured and simulated relative beam content for pions and muons for 1 and 3 GeV/c. The 6 GeV/c data point was obtained using the copper target, and also includes the positrons that cannot be distinguished from pions and muons for momenta ≥ 4 GeV/c. Data and simulations are in satisfactory agreement.

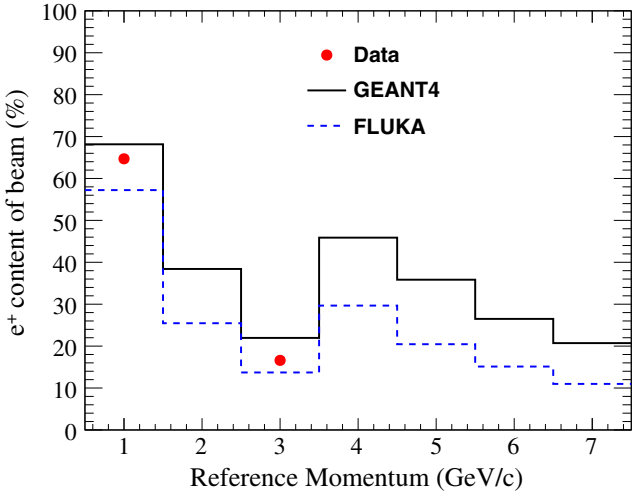

FIG. 22. Measured and simulated beam content for positrons. Data were only taken for 1 GeV/c and 3 GeV/c, using the W target. A quite satisfactory agreement with the simulations is demonstrated, with the differences in the beam composition not exceeding 20 % between the data and the average of the two Monte-Carlo programs.

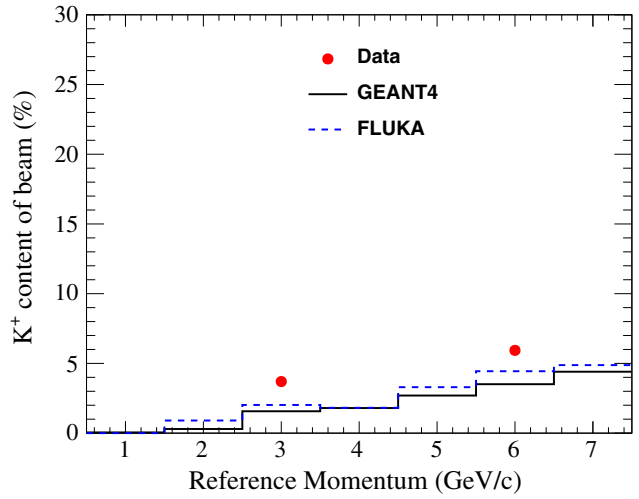

FIG. 23. Measured and simulated beam content for kaons. Data were only taken for 3 and 6 GeV/c, using the W target for 3 GeV/c and the Cu target for 6 GeV/c. A satisfactory agreement is demonstrated, since the data seem to agree within a maximum of factor of two with the simulations, at 3 GeV/c, while an even better agreement is observed at 6 GeV/c.

The beam composition has been also measured using the PID scheme described in the previous sections. Due to the fact that these measurements took place outside the beam commissioning period, in parallel with the physics program of the experiment, only data in certain momenta were recorded, following the experimental requirements. The results, for the pion and muon content at momenta below 4 GeV/c and for the sum of pions, muons and positrons in the range of 4–7 GeV/c are shown in Fig. 21, where a satisfactory agreement within 20 % between the average of the counts given by both Monte-Carlo codes and the data is demonstrated.

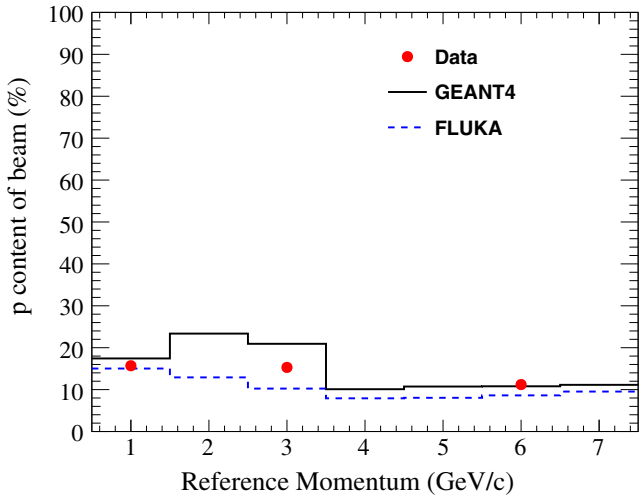

FIG. 24. Measured and simulated beam content for protons. A very good agreement between measurements and simulations is also present.

A similar analysis was done for positrons. The results are shown in Fig. 22. For momenta above 4 GeV/c a distinction between positrons and pions was not possible with the current PID schema. Instead, the kaons at 3 and 6 GeV/c could be identified (Fig. 23). Also here, a very good agreement with the simulations is shown, with the measured relative composition percentage of kaons not exceeding a factor of two compared with the simulated one.

The same comparison for protons is shown in Fig. 24. Once more, a satisfactory agreement is demonstrated between data and the two Monte-Carlo simulation programs.

V. SUMMARY AND DISCUSSION

The production, transport, and identification of particles in the hadron momentum regime of interest for neutrino physics of 1–7 GeV/c was presented and discussed. The H4-VLE beam line optics were optimized towards the maximization of angular acceptance and the treatment of possible misalignments. We have demonstrated that MAD-X and PTC are suitable tools for acceptance maximization and misalignment studies in low energy beam lines, being superior to older optics and tracking codes due to the extra features offered, like the customization of output formats and the convenient variable communication between optics and tracking modules. The comparison of the tracking results with G4beamline did not show any discrepancy between the two codes, thus validating the approach. At the same time, the background at the detector was reduced with nonstandard shielding design (using the well established, for similar studies, FLUKA code). Novel instrumentation consisting of scintillating fiber detectors in two different read-out configurations was developed and commissioned, the performance of which has been analyzed and discussed in this paper. Different particle identification techniques, including time-of-flight and threshold Cherenkov detectors used in conjunction with timing of each trigger event, allowed for full identification of individual particles in the desired momentum range, on an event-by-event basis.

The measured trigger rate and beam composition are in good agreement (∼20 %) with both FLUKA and G4beamline (using the FTFP_BERT physics list). Given the differences in the various particle species production (in terms of total and relative rate as well as phase-space coordinates) between the Monte-Carlo programs, we consider this agreement very satisfactory. The total measured trigger rates at all momenta are well above the detector DAQ capabilities, and within the original design specifications of the beam line. A momentum measurement with a resolution of ∼2.5 % is provided through the XBPF-based spectrometer. It has been moreover demonstrated that 10^6 particles with a relatively good ($\geq$ 50 %) pion content, with an initial energy of 80 GeV/c impinging on a thick target, given a suitable, large acceptance, magnetic spectrometer beam

line design, can provide a satisfactory rate of relatively low energy hadrons and leptons, useful for current and future neutrino detector R&D, as well as for other high-energy physics and beam applications. The electron or positron content can be suppressed using a higher-Z target material, like tungsten. The minimization of material budget is crucial for avoiding particle loss, extra momentum spread and emittance growth. A moderate time-of-flight (sub ns) system is sufficient for identifying the low momentum particles, while a combination of two threshold Cherenkov counters, using CO_2 as radiator gas, allows tagging of the different particle species. Operating one Cherenkov detector at low pressure (≤ 5 bar) and a second one at higher pressures (up to 15 bar) allows for flexibility and provides the possibility to further reduce the material budget, when necessary, by emptying one of the two detectors to a sub-bar pressure. The scintillating fiber detectors have also proven to be ideal for profile measurements and to act additionally as trigger counters, allowing for a large surface coverage and very low material budget, combined with an excellent efficiency of 95 %.

ACKNOWLEDGMENTS

The authors would like to thank L. Gatignon, I. Efthymiopoulos and N. Doble for useful discussions on the beam line design and the instrumentation. The Neutrino Platform and NP-04 teams are gratefully acknowledged for their flexibility during the beam line commissioning. In addition the authors would like to thank the technical and engineering staff of CERN EN-EA group (S. Girod, A. E. Rahmoun, B. Rae, V. de Jesus, E. Grospelier, B. Pellegrinelli, M. Jeckel and E. Harrouch), CERN EN-HE group (S. Pelletier, F. Daclin and N. Debiee), CERN EN-SMM group (P. Dewitte, D. Mergelkuhl, K. Nikolitsas) and CERN TE-MSC group (P. Schwarz) for their dedication during the beam line installation and first operation. The help of CERN BE-CO (M. Hrabia, M. Gabriel) for the necessary beam controls optimization, and CERN BE-BI colleagues for the tuning of the instrumentation (P. Carriere, A. Frassier, S. Dechamps, W. Devauchelle and J. Fullerton) is also very much appreciated. The guidance of F. Schmidt (CERN, BE-ABP) through the particularities of MAD-X and PTC codes is gratefully acknowledged. A. C. B. acknowledges the Science and Technology Facilities Council (STFC) - reference: ST/R505146/1 for providing the funding for his research. The authors would finally like to thank M. Brugger (CERN, EN-EA) for his overall support to the project.

[1] CERN Secondary Beam Areas https://sba.web.cern.ch/sba/.
[2] H. Atherton, C. Bauvet, N. Doble, L. Piemontese, A. Placci, D. Plane, M. Reinharz, E. Rossa, and G. V. Holtey, Precise measurements of particle production by 400 GeV/c protons on beryllium targets, CERN Yellow Report No. 80-07.
[3] G. Ambrosini *et al.* (The NA56/SPY Collaboration), Measurement of charged particle production from 450 GeV/c protons on beryllium, Eur. Phys. J. C **10**, 605 (1999).
[4] B. Abi *et al.*, The single-phase protodune technical design report, arXiv:1706.07081.
[5] S. Bertolucci *et al.*, Memorandum of understanding for providing a framework for developing a neutrino program at CERN, CERN EDMS Server, http://cenf.web.cern.ch/.
[6] B. Abi *et al.*, Long-Baseline Neutrino facility (LBNF) and Deep Underground Neutrino Experiment (DUNE), arXiv:1601.05471.
[7] N. Charitonidis and I. Efthymiopoulos, Low energy tertiary beam line design for the CERN neutrino platform project, Phys. Rev. Accel. Beams **20**, 111001 (2017).
[8] K. Brown, D. Carey, C. Iselin, and F. Rothacker, TRANSPORT: A computer program for designing charged particle beam transport systems, CERN Report No. 80-04.
[9] D. Carey, K. Brown, and C. Iselin, Decay TURTLE, trace unlimited rays through lumped elements: A computer program for simulating charged particle beam transport systems, including decay calculations, Report No. SLAC-246, 1982.
[10] T. J. Roberts, K. Beard, D. Huang, S. Ahmed, D. M. Kaplan, and L. Spentzouris, G4beamline: Particle tracking in matter dominated beam lines, in *Proceedings of the 11th European Particle Accelerator Conference, Genoa, 2008* (EPS-AG, Genoa, Italy, 2008), WEPP120.
[11] R. Brun and F. Rademakers, ROOT—An object oriented data analysis framework, Nucl. Instrum. Methods Phys. Res., Sect. A **389**, 81 (1997).
[12] Wolfram Research Inc, Mathematica, version 12.0, Champaign, IL, 2019.
[13] Methodical Accelerator Design CERN, http://mad.web.cern.ch/mad/.
[14] P. Skowronski and F. Schmidt, Advances in MAD-X using PTC, in *Proceedings of the 22nd Particle Accelerator Conference, PAC-2007, Albuquerque, NM* (IEEE, New York, 2007), THPAN070.
[15] P. Chatzidaki, Optics optimization of tertiary particle beamlines and efficiency measurement of prototype scintillating fiber detectors, Diploma thesis, National Technical University of Athens, http://cds.cern.ch/record/2666202?ln=en.
[16] E. Forest, S. C. Leemann, and F.Schmidt, Fringe effects in MAD PART I, Second order fringe in MAD-X for the module PTC, http://frs.web.cern.ch/frs/report/fringe_part_I.pdf.
[17] Kilean Hwang and S. Y. Lee, Dipole fringe field thin map for compact synchrotrons, Phys. Rev. ST Accel. Beams **18**, 122401 (2015).
[18] OPERA3D reference manual, VF-09-99-B2.
[19] T. Böhlen, F. Cerutti, M. Chin, A. Fassò, A. Ferrari, P. Ortega, A. Mairani, P. Sala, G. Smirnov, and V. Vlachoudis, The FLUKA code: Developments and challenges for high energy and medical applications, Nucl. Data Sheets **120**, 211 (2014).
[20] A. Ferrari, P. Sala, A. Fassò, and J. Ranft, FLUKA: A multi-particle transport code, Reports No. CERN-2005-10, 2005, No. INFN/TC 05/11, No. SLAC-R-773.

[21] I. Ortega, Accurate profile measurement of the low intensity secondary beams in the cern experimental areas, Ph.D. thesis, Ecole Polytechnique Federale de Lausanne (EPFL), THESE No. 8278, 2018, https://infoscience.epfl.ch/record/253109?ln=en.

[22] The White Rabbit Project https://ohwr.org/project/white-rabbit/wikis/home.

[23] ANSI/VITA 58.0-2009 (R2014), https://www.vita.com/Standards.

[24] N. Charitonidis, Y. Karyotakis, and L. Gatignon, Estimation of the R134a gas refractive index for use as a Cherenkov radiator, using a high energy charged particle beam, Nucl. Instrum. Methods Phys. Res., Sect. B **410**, 134 (2017).

[25] A. Bideau-Mehu, Y. Guern, R. Abjean, and A. Johannin-Gilles, Interferometric determination of the refractive index of carbon dioxide in the ultraviolet region, Opt. Commun. **9**, 432 (1973).

[26] N. Charitonidis, I. Efthymiopoulos, and Y. Karyotakis, Beam performance and instrumentation studies for the ProtoDune-DP experiment of CENF, Report No. CERN-ACC-NOTE-2016-0052, http://cds.cern.ch/record/2202366?ln=en.

[27] M. Aharrouche *et al.*, Measurement of the response of the ATLAS liquid argon barrel calorimeter to electrons at the 2004 combined test-beam, Nucl. Instrum. Methods Phys. Res., Sect. A **614**, 400 (2010).

[28] N. Charitonidis, I. Efthymiopoulos, and Y. Karyotakis, Addendum to ATS Reports No. CERN-ACC-NOTE-2016-0052, No. CERN-ACC-NOTE-2016-0059, https://cds.cern.ch/record/2224290?ln=en.